



## Phase constitution and glass formation in an Au-based alloy

Gianluca Fiore\*, Paola Rizzi, Livio Battezzati

Dipartimento di Chimica IFM e Centro di Eccellenza NIS, Universit'a di Torino, Via P. Giuria 9, 10125 Torino, Italy

### ARTICLE INFO

#### Article history:

Received 3 July 2010

Received in revised form 17 January 2011

Accepted 18 January 2011

Available online 1 February 2011

#### Keywords:

Metallic glasses

Gold-base

Crystallization

Transformation diagrams

### ABSTRACT

Studies on the phase constitution of annealed master ingots of the  $\text{Au}_{49}\text{Ag}_{5.5}\text{Pd}_{2.3}\text{Cu}_{26.9}\text{Si}_{16.3}$  alloy suggest that it is a quinary eutectic and revealed which phases solidify from the melt. The alloy has been amorphized in ribbon form. Ribbon crystallization has been studied in isothermal and continuous heating modes. From such experiments data on the mechanism and kinetics of crystallization have been obtained. Time–temperature–transformation and Continuous Heating Transformations plots for crystallization have been derived from thermal data.

© 2011 Elsevier B.V. All rights reserved.

### 1. Introduction

The discovery of a Au-based metallic glass with nominal composition  $\text{Au}_{49}\text{Ag}_{5.5}\text{Pd}_{2.3}\text{Cu}_{26.9}\text{Si}_{16.3}$  (at.%) [1] has suggested its use as a material for jewelry, as well as for hi-tech devices like micro-electromechanical system (MEMS) [2] thanks to a good workability in the undercooled liquid regime [2–4], good mechanical properties [5], high hardness values (360 HV) compared to conventional gold alloys (~250 HV) [6] and a gold content equal to 18-karat.

Metallic glasses can be processed in the undercooled liquid regime. Here the alloys behave like a Newtonian fluid and can fill cavities, adapt to surface features, and be shaped in complex forms [7]. Due to the metastable nature of the undercooled liquid, the time available for processing is limited by the time to reach crystallization.

The time–temperature–transformation (TTT) diagram is a useful tool for comparing thermal stabilities of different glasses, as well as for the selection of heat treatment.

In the present work a TTT plot for the start and the end of the crystallization of  $\text{Au}_{49}\text{Ag}_{5.5}\text{Pd}_{2.3}\text{Cu}_{26.9}\text{Si}_{16.3}$  is obtained from isothermal differential calorimetry data. In addition a continuous heating transformation (CHT) plot is given together with accounts on the phases responsible for crystallization.

### 2. Experimental

The master alloy with nominal composition  $\text{Au}_{49}\text{Ag}_{5.5}\text{Pd}_{2.3}\text{Cu}_{26.9}\text{Si}_{16.3}$  (named A5) was prepared by arc-melting the pure elements in Ar atmosphere with Ti and Zr getters.

Ribbon samples 2–3 mm wide and some tens of micron thick were obtained in a melt spinning apparatus under Ar atmosphere, the velocity of the wheel was 22 m/s.

The structure of the samples was examined by X-ray diffraction (XRD) with monochromatic  $\text{Cu K}\alpha$  radiation. Phase transformations were studied by differential scanning calorimetry (DSC); different heating rates were employed in order to study the crystallization process of the amorphous phase. All DSC runs were performed under flowing Ar. The calorimeter cell was calibrated, at each heating rate, by recording the melting temperatures and the heats of fusion of In and Zn. The microstructure of the master alloy was investigated with scanning electron microscopy (SEM) and phases composition was checked by energy dispersive X-ray spectroscopy (EDS).

### 3. Results and discussion

Although bulk glasses are easily produced with the present alloy [8], this study has been performed using ribbons to ensure full amorphization in all part of the material and to use smaller samples. The amorphicity of the ribbons is confirmed by XRD analysis (not reported here) giving patterns with the presence of only halo reflections. Calorimetric traces of the as spun ribbons heated at different rates are reported in Fig. 1(a–d). The first thermal data of the as spun ribbon were collected in February 2008 when it was spun. Its DSC trace (Fig. 1b), performed at 20 °C/min, shows a clear glass transition followed by a wide undercooled liquid region and then crystallization. The data used for this work have been collected two years after the sample preparation and a thermal characterization of the “aged” ribbon has been repeated and is shown in Fig. 1c. By comparison with the as spun sample (Fig. 1b) it noted that the end temperature of the glass transition ( $T_{g,\text{end}}$ ) does not change, but an endothermic peak appears just below the glass transition range (see arrows of Fig. 1c and inset). From the literature, the nature of such peak can be associated with the disruption of chemical short range order (CRSO) introduced by annealing the sample well below the glass transition temperature ( $T_g$ ) [9,10]. In this case ageing means

\* Corresponding author. Fax: +39 0116707855.

E-mail address: [gianluca.fiore@unito.it](mailto:gianluca.fiore@unito.it) (G. Fiore).

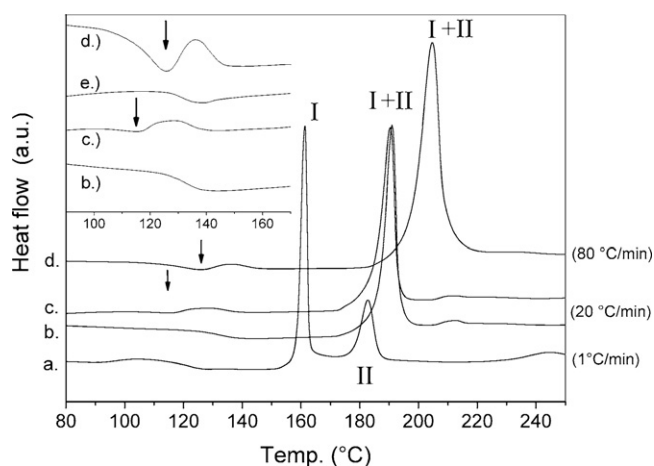


**Fig. 1.** DSC traces at different heating rates of the rapidly solidified samples: (a) aged sample scanned at 1 °C/min; (b) as spun sample scanned at 20 °C/min; (c) aged sample scanned at 20 °C/min; (d) aged sample scanned at 80 °C/min.

that the sample stayed at room temperature over the seasons. A further scan at 80 °C/min highlights the presence of the endothermic peak (Fig. 1d and inset).

Crystallization peaks of the as spun (Fig. 1b) and aged (Fig. 1c) samples do not show any difference in onset temperature and shape and their crystallization heats are comparable being  $20.1 \pm 0.4$  J/g and  $20.4 \pm 0.4$  J/g, respectively.

Thermal analysis has been performed in scanning and isothermal conditions. In the first case the amorphous ribbon has been heated at low heating rate (1 °C/min) up to the end of melting. Transformations of the ribbon take place in several steps. In this work we have reported only data concerning the first two peaks (peaks I and II of Fig. 1) since the devitrification of the amorphous matrix is already completed when the end of the first crystallization peak is reached (Fig. 2a). The heat involved in the first transformation is  $12.7 \pm 0.4$  J/g, and the second one is  $6.3 \pm 0.3$  J/g. The sum of the two matches the heat values obtained at 20 °C/min for the single “I + II” peak which apparently is the result of the merging of the two exothermic events seen at low rates.

At the end of each transformation at low heating rate we have collected diffraction patterns (Fig. 2a and d) where no evidence of residual amorphous halo appears. Such patterns have been used as

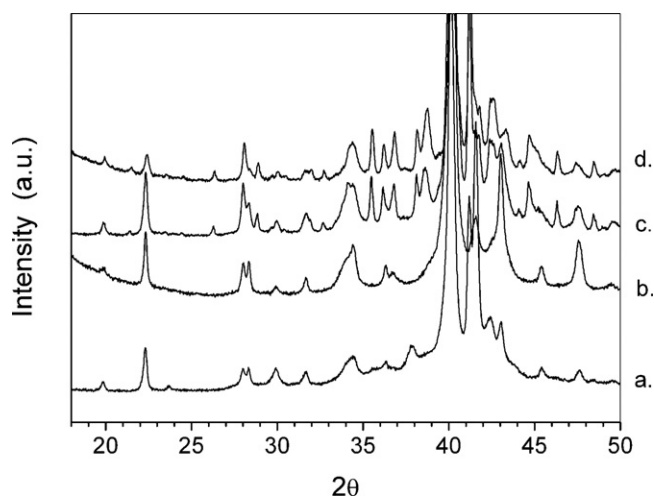


**Fig. 2.** XRD patterns of the samples crystallized in heating and isothermal modes: (a) sample scanned (1 °C/min) up to 165 °C (I peak); (b) sample isothermally crystallized at 170 °C; (c) sample scanned (1 °C/min) up to 190 °C (II peak); (d) sample crystallized isothermally and then scanned up to the end of the peaks of Fig. 5.

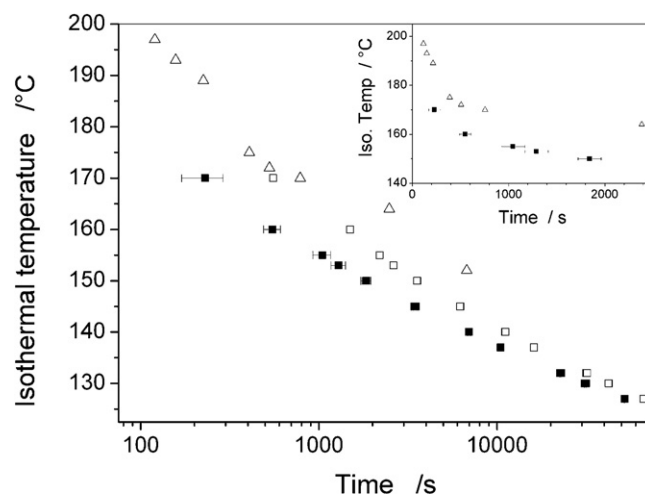


**Fig. 3.** TTT and CHT plots. Close and open squares are related to the onset and the end of the isothermal crystallization, respectively. Open triangles refer to the onset of the peak in CHT.

reference for the structural characterization of the phases obtained from isothermal experiments.

The isothermal crystallization was performed by annealing the samples at different temperatures ( $T_a$ ) in the range 127–170 °C until an exothermic calorimetric signal is completely manifested. The annealing temperatures ( $T_a$ ) were reached at 80 °C/min.

The isothermal crystallization heats are comparable with those obtained at low scanning rate. This shows that the isothermal transformation corresponds to the first peak on continuous heating.

In Fig. 3 the times required for reaching the onset (close squares) and the end (open squares) of the crystallization at each isothermal temperature are reported giving as result a TTT plot. Open triangles refer to the onset of the peak in continuous heating transformations (CHT). The data show that the alloy has good stability against crystallization leaving sufficient time for processing it in the undercooled liquid region.

Reaching the annealing temperatures in the  $T_g$  range at 80 °C/min implies that structural relaxation is not completed yet (Fig. 1d inset). When the isothermal regime is reached a very minor heat effect, not interfering with crystallization is recorder. Note that a sample previously heated above  $T_g$ , cooled, and then annealed at 127 °C gave the same results as the quenched one.

The early stage of crystallization involves the nucleation of a simple cubic phase with lattice parameter equal to 8.96 Å; during a further transformation the structure of this phase changes decreasing its symmetry as suggested by the splitting of some peaks (Fig. 4) (see at about 28° for the sample annealed at 170 °C). The phase can be indexed approximately with reflection behaving to the “Cu<sub>83</sub>Si<sub>17</sub>” structure [11].

The phases of the annealed samples have been studied by means of XRD analysis. Patterns are collected in Fig. 4. From the top (annealed at 127 °C) to the bottom (annealed at 170 °C) it is noted that increasing the annealing temperature ( $T_a$ ) some peaks appear and grow in intensity meanwhile others disappear.

The diffraction pattern of the sample annealed at 170 °C shows the same phases that appear in the sample scanned at low heating rate (1 °C/min) up to the end of the first crystallization peak (Fig. 2a and b).

After isothermal crystallization samples were scanned at 80 °C/min in order to check for the presence of residual crystallization after the first signal. At the lower annealing temperatures the thermogram consist of two overlapping signals. As  $T_a$  increases the signals tend to merge shifting the maximum of the peak to lower temperature (Fig. 5). Although their shapes are different, they give

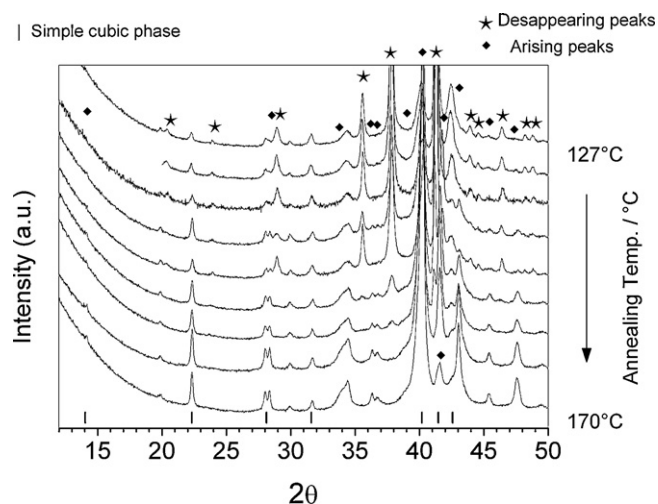


Fig. 4. XRD patterns of the samples crystallized isothermally at the annealing temperatures reported in Fig. 3.

the same enthalpy value:  $6.5 \pm 0.3$  J/g which is comparable with the heat of peak II obtained in scanning mode, suggesting that the transformation corresponds to the second peak of Fig. 1a. In order to confirm this we have compared the diffraction pattern given by those samples with that obtained after scanning at  $1^\circ\text{C}/\text{min}$  up to the end of peak II (Fig. 2c) finding fully correspondence (Fig. 2c and d).

Both isothermal and scanning data have been used for calculating the activation energy ( $E_a$ ) for the crystallization process in an Arrhenius and Kissinger plot, respectively. Their values are  $177 \pm 4$  kJ/mol and  $162 \pm 3$  kJ/mol [12], respectively, and they are comparable with activation energy data of chemical diffusion in Au–Cu crystalline alloys [13].

In order to obtain the equilibrium phases a portion of the alloy was cycled two times above the liquidus temperature, then heated up to eutectic peak temperature, annealed for 5 min and then slowly cooled. The microstructure of the sample (Fig. 6) is constituted by five phases: the matrix consists by two silicides rich in Au (light grey phase) and Cu (grey phase), respectively, in which Ag and either Cu or Au are partially dissolved. The circled phase is identified with free Si; the dark phase is apparently a Pd silicide containing some Au and Cu. The fifth phase (white arrows) is a Au rich solid solution containing Ag and Cu.

In Fig. 7 the diffraction pattern of the sample is reported. The Au-rich silicide can be referred to the “Au<sub>5</sub>Si” structure. The dark

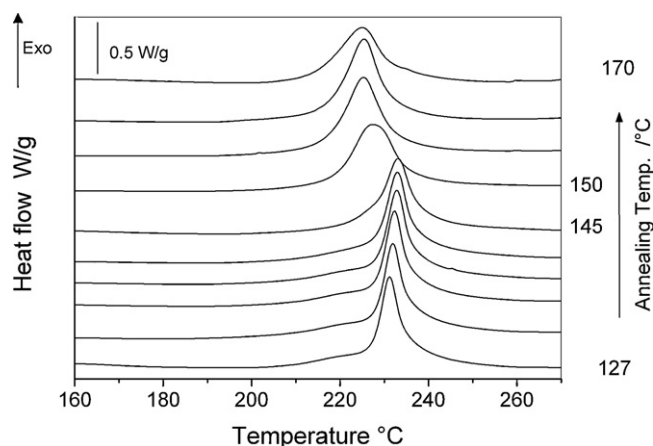


Fig. 5. Continuous heating traces (at  $80^\circ\text{C}/\text{min}$ ) of the samples previously annealed in the range  $127$ – $170^\circ\text{C}$ .

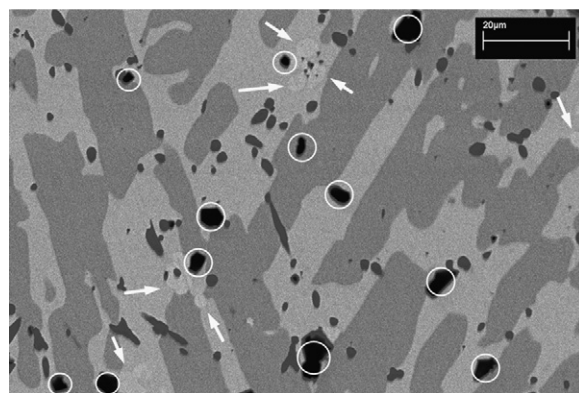


Fig. 6. Backscattered electron (BE) images of the master alloy thermally treated in order to obtain the equilibrium phases.

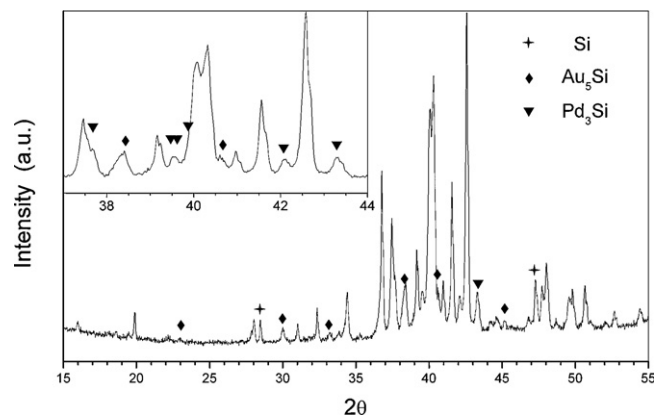


Fig. 7. XRD pattern of the master alloy thermally treated in order to obtain the equilibrium phases.

phase is very likely Pd<sub>3</sub>Si with lattice parameter slightly modified due to the presence of Au and Cu. The Cu-rich silicide could not be identified. Its XRD reflections do not match any of the known phase types (e.g. Cu<sub>15</sub>Si<sub>4</sub> [14], Cu<sub>83</sub>Si<sub>17</sub> [11], Cu<sub>5</sub>Si [15] and Cu<sub>4</sub>Si [16]). It is noted that the transformations occurring after crystallization are due to phase changes of Cu-silicides, from the metastable cubic phase to the unknown phase mentioned above.

#### 4. Conclusions

The thermal stability of the Au<sub>49</sub>Ag<sub>5.5</sub>Pd<sub>2.3</sub>Cu<sub>26.9</sub>Si<sub>16.3</sub> alloy has been investigated studying the crystallization process in isothermal and scanning mode. From such data a TTT and CHT plot have been obtained showing that the alloy has good stability against crystallization and providing time for processing the alloy in its undercooled liquid region of the order of several minutes. The early stage of the devitrification of the amorphous matrix involves the nucleation of a simple cubic phase with lattice parameter equal to 8.96 Å. Crystallization at low scanning rate ( $1^\circ\text{C}/\text{min}$ ) shows the splitting of the main crystallization peak observed at conventional heating rate ( $20^\circ\text{C}/\text{min}$ ) and it is completed when the end of the first crystallization peak is reached.

The equilibrium microstructure of the master alloy is constituted by five phases: “Au<sub>5</sub>Si” type, Si, Au-rich solid solution, Pd<sub>3</sub>Si and a Cu-rich silicide that have not been identified yet. None of these forms directly from the amorphous phase whose stability is limited by the formation of metastable Cu-based silicides.

## Acknowledgements

Work performed for PRIN, 2008. Fondazione S. Paolo is acknowledged for support to CdE NIS.

## References

- [1] J. Schroers, B. Lohwongwatana, W.L. Johnson, A. Peker, *Appl. Phys. Lett.* 87 (2005) 061912.
- [2] J. Schroers, T. Nguyen, S. O'Keefe, A. Desai, *Mater. Sci. Eng. A: Struct.* 449–451 (2007) 898–902.
- [3] J. Schroers, Q. Pham, A. Peker, N. Paton, R.V. Curtis, *Scr. Mater.* 57 (2007) 341–344.
- [4] G. Kumar, H.X. Tang, J. Schroers, *Nature* 457 (2009) 868–872.
- [5] N. Li, L. Liu, K.C. Chan, Q. Chen, J. Pan, *Intermetallics* 17 (2009) 227–230.
- [6] J. Schroers, B. Lohwongwatana, W.L. Johnson, A. Peker, *Mater. Sci. Eng. A: Struct.* 448–451 (2007) 235–238.
- [7] G. Fiore, L. Battezzati, *Adv. Eng. Mater.* 9 (2007) 509–511.
- [8] G. Fiore, I. Ichim, L. Battezzati, *J. Phys. Conf. Ser.* 144 (2009) 012039.
- [9] H.S. Chen, *J. Non-Cryst. Solids* 46 (1981) 289–305.
- [10] L. Battezzati, G. Riontino, M. Baricco, A. Lucci, F. Marino, *J. Non-Cryst. Solids* 61–62 (1984) 877–882.
- [11] JCPDS card number 00-023-0223.
- [12] G. Fiore, I. Ichim, L. Battezzati, *J. Non-Cryst. Solids* 356 (2010) 2218–2222.
- [13] C.J. Smithells, *Metals Reference Book*, Butterworth, 1976.
- [14] JCPDS card number 01-076-1800.
- [15] JCPDS card number 00-004-0841.
- [16] JCPDS card number 00-003-0990.